

Supplementary Materials

Exploring the pH-induced Functional Phase Space of Human Serum Albumin by EPR Spectroscopy

Jörg Reichenwallner ¹, Marie-T. Oehmichen ¹, Christian E. H. Schmelzer ^{2,3}, Till Hauenschild ¹,
Andreas Kerth ¹, Dariush Hinderberger ^{1,*}

¹Institute of Chemistry, Martin Luther University Halle-Wittenberg, Von-Danckelmann-Platz 4, 06120 Halle (Saale), Germany; joerg.reichenwallner@chemie.uni-halle.de (J.R.); marie-therese.oehmichen@student.uni-halle.de (M.T.O); till.hauenschild@chemie.uni-halle.de (T.H.); andreas.kerth@chemie.uni-halle.de (A.K.).

²Institute of Pharmacy, Martin Luther University Halle-Wittenberg, Wolfgang-Langenbeck-Strasse 4, 06120 Halle (Saale), Germany; schmelzer@pharmazie.uni-halle.de (C.E.H.S)

³Fraunhofer Institute for Microstructure of Materials and Systems IMWS, Walter-Hülse-Strasse 1, 06120 Halle (Saale), Germany.

*Correspondence: dariush.hinderberger@chemie.uni-halle.de (D.H.); Tel.: +49-345-55-25230

Contents

S1 Results from MALDI-ToF Experiments on 5-MSL HSA	p. 2
S2 Data Extraction from CW EPR Spectra	p. 2
S3 Collective Lysine pK _a Estimation from pH-dependent EPR Experiments (5-MSL HSA)	p. 5
S4 Exemplary Simulation of 16-DSA Alone and Interacting with HSA	p. 6
S5 Rationalization and Analyses of I_{abf} Curves	p. 7
S6 Analysis of pH-dependent Apparent Hyperfine Coupling Constants $A_{ }$	p. 10
S7 Determination of Low Temperature A_{zz} Values at $T = 150$ K from Spin Probed HSA	p. 11
S8 Analysis of $\Delta B_{0,pp}$ Curves	p. 12
S9 Further Information about Order Parameters S and Wobbling Angles γ	p. 14
S10 Shift of $P_{max}(r)$ in DEER Data from pH Denaturation of 16-DSA Spin Probed HSA	p. 16
S11 Functional Phase Space of HSA as Obtained from EPR Spectroscopy and DLS	p. 17
S12 Supplementary References	p. 18

S1 | Results from MALDI-ToF Experiments on 5-MSL HSA

The molecular weights of HSA and spin-labeled 5-MSL HSA samples are shown in Figure S1. The weight increase of HSA is shown for two independent labeling procedures and amounts to $\Delta MW_1 = +639$ Da and $\Delta MW_2 = +849$ Da. With $MW_{5\text{-MSL}} = 237.27$ Da. This corresponds to a degree of modification of $n_1 = \Delta MW_1 / MW_{5\text{-MSL}} = 2.69$ and $n_2 = \Delta MW_2 / MW_{5\text{-MSL}} = 3.58$. Thus, on average $n_{\text{MSL}} = 3.14 \pm 0.45$ spin labels are covalently attached to HSA during a 5:1 incubation procedure as it was applied here.

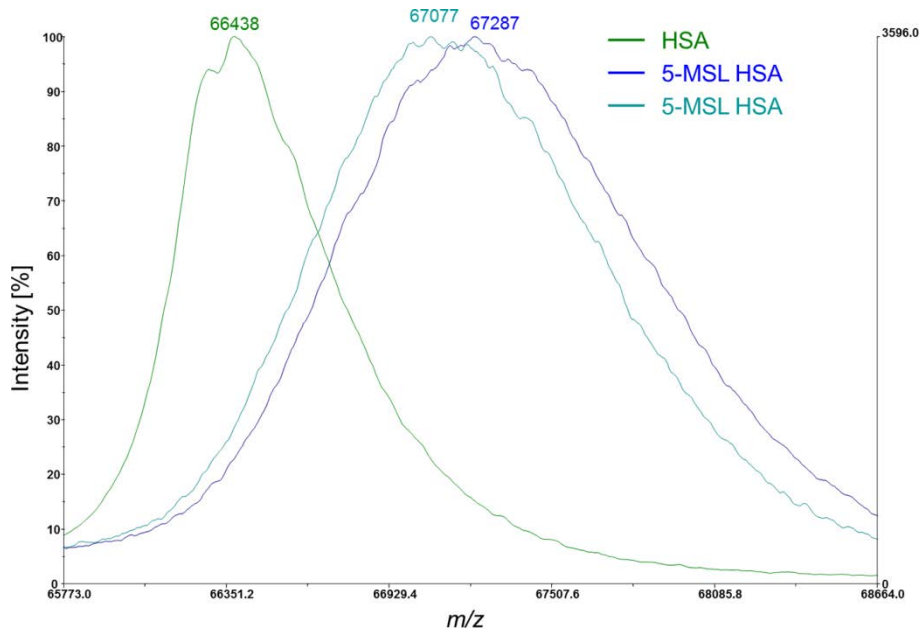


Figure S1. Molecular weights of HSA and 5-MSL HSA. The spectrum shows the overlaid peaks of HSA (green) and 5-MSL HSA (cyan and blue) with the derived masses of their singly charged ions $[M+H]^+$. Maximum intensities were normalized to 100% for clarity.

S2 | Data Extraction from CW EPR Spectra

In order to extract apparent hyperfine coupling constants $A_{//}$ [S1] and collective rotational correlation times τ_c from CW EPR spectra of 5-MSL HSA, a scheme is presented in Figure S2 of how corresponding data in Figure 2b were obtained. According to a strategy presented by Meirovitch and Freed [S2] the A -tensor components (A_{xx} , A_{yy} , A_{zz}) are extracted from low-temperature X-band CW EPR spectra (A_{zz}) in combination with room temperature spectra (a_{iso}), assuming an overall axial nitroxide geometry with $A_{xx} = A_{yy}$. The pure A_{zz} tensor value can be extracted from CW EPR spectra below about 200 K, as the strongly restricted rotational freedom leads $A_{//}$ to approach A_{zz} [S3]. This is the characteristic threshold temperature when intramolecular motions with $\tau_c < 100$ ns become visible from an e.g. protein sample. The isotropic hyperfine coupling constant:

$$a_{\text{iso}} = \text{Tr}(\mathbf{A}) = \frac{1}{3}(A_{xx} + A_{yy} + A_{zz}) = \frac{1}{3}(2A_{xx} + A_{zz}) \quad (\text{S1})$$

from 5-MSL is here taken from an extremely basic room temperature sample at pH 11.96, where the freely rotating component with its typical three-line spectra is dominant and clearly identifiable. Figure S2a shows the spectral positions of specific features that were extracted ($x_i \in A_i, a_i$). However, besides the straightforward peak-picking procedure, a Manganese standard (Magnettech GmbH) has been used to take device-specific uncertainties in relative line-positions into account and a sweep-width correction factor $k_{SW} = 0.9965$ could be determined for experiments with the 5-MSL spin label and $k_{SW} = 0.9923$ for 5-DSA and 16-DSA (average value: $k_{SW} = 0.9944$). The corrected values for A_{zz} , $A_{||}$ and a_{iso} are therefore generally obtained with following expression:

$$x = \frac{k_{SW}}{2}(B(x_2) - B(x_1)) \quad , \quad (S2)$$

where $B(x_i)$ are the corresponding magnetic field positions in Gauss [G]. Errors for A_{zz} and $A_{||}$ are determined by the relation (Figure S2b):

$$\Delta x = \frac{k_{SW}}{2}(\Delta B(x_2) + \Delta B(x_1)) \quad , \quad (S3)$$

as obtained from the propagation of uncertainty. The respective error in individual $\Delta B(x_i)$ are determined during data readouts (e.g. here in Figure S2: $\Delta A_{zz} = 0.20$ G).

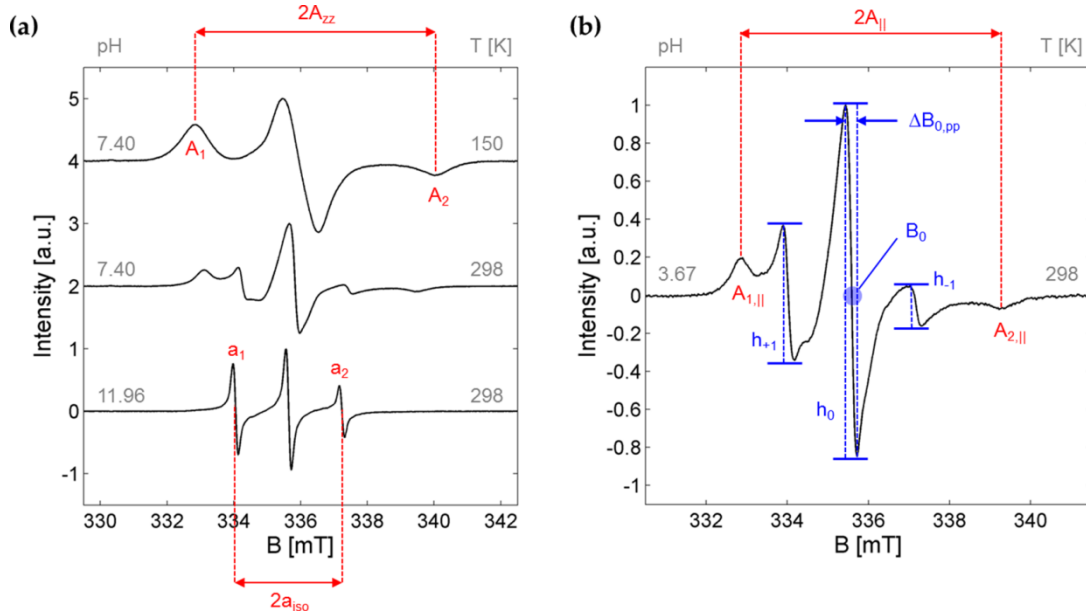


Figure S2. Exemplary data extraction from CW EPR spectra of 5-MSL HSA. (a) Determination of A_{zz} from peak positions A_i in a $T = 150$ K low temperature spectrum of 1.35 mM 5-MSL HSA in DPBS buffer pH 7.4 (top lane), directly after the concentration step of the purification procedure. The a_{iso} value is taken from value (a_i) of a 0.09 mM 5-MSL HSA sample at pH 11.96 with clearly distinguishable isotropic three-line components of 5-MSL (bottom lane, room temperature, $T = 298$ K). Additionally, a room temperature spectrum of the sample in the top lane is shown in the middle lane. (b) Determination of $A_{||}$ from peak positions $A_{i,||}$ in a room temperature spectrum of 0.09 mM 5-MSL HSA at pH 3.67. The parameters h_{+1} , h_0 , h_{-1} , B_0 and $\Delta B_{0,pp}$ are extracted for calculations of collective rotational correlation times τ_c (see equations S8 and S9).

Furthermore, this strategy was pursued for all manual data extraction procedures in this study (x -axis values derived from 5-DSA and 16-DSA spectra are: A_{\parallel} , A_{\perp} , A_{zz} , $\Delta B_{0,pp}$, see Figure 4a). The error for a_{iso} is related to the magnetic field resolution $\Delta B(x_i) = B_{max}/N_{max} = 3.66 \mu\text{T} = 0.0366 \text{ G}$ with $B_{max} = 15 \text{ mT}$ being the sweep width and the number of recorded data points $N_{max} = 4096$, so that $\Delta a_{iso} = k_{SW} \cdot \Delta B(a_i) = 0.0365 \text{ G}$. If necessary, values and their errors for y -axis values (e.g. h_0 , h_{\perp} and h_{-1} , see Figure 4a) were extracted with:

$$y = \frac{1}{2}(y_2 - y_1) \quad (\text{S4})$$

and
$$\Delta y = \frac{1}{2}(\Delta y_2 + \Delta y_1) \quad (\text{S5})$$

According to the method from Meirovitch [S2], equations S1 – S3 can be combined to yield an expression for A_{xx} and A_{yy} :

$$A_{xx} = A_{yy} = \frac{k_{SW}}{4} (3 \cdot (B(a_2) - B(a_1)) - (B(A_2) - B(A_1))) = \frac{k_{SW}}{2} (3 \cdot a_{iso} - A_{zz}) \quad (\text{S6})$$

with the uncertainties:

$$\Delta A_{xx} = \Delta A_{yy} = \frac{k_{SW}}{4} (6\Delta B(a_i) + \Delta B(A_2) + \Delta B(A_1)) \quad (\text{S7})$$

Finally, the A -tensor values of 5-MSL can be determined as $A_{zz} = (35.78 \pm 0.20) \text{ G}$, $A_{xx} = A_{yy} = (5.91 \pm 0.13) \text{ G}$ and $a_{iso} = (15.863 \pm 0.037) \text{ G}$. The well-known semi-empirical approach for calculations of pH-dependent rotational correlation times τ_c was also tested [S4,S5]. As multicomponent CW EPR spectra can be observed throughout all pH values for 5-MSL HSA, the precise extraction of individual rotational components is only accessible by thorough spectral simulation. Therefore, the calculated values are termed as collective rotational correlation times τ_c . The magnetic parameters for g - and A -tensors were used, with the former one being regarded as principally inaccessible without simulations at X-Band frequencies. Therefore, the g -tensor values given in Marzola *et al.* [S6] with $g_{xx} = 2.0084$, $g_{yy} = 2.0061$, $g_{zz} = 2.0025$ were used here. Explicit formulae from lineshape theory are given in equation S8 and S9. Furthermore, the τ_c values are usually obtained by calculating the arithmetic average of both values $\tau_{c,1}$ and $\tau_{c,2}$ that are defined as [S4,S5,S7]:

$$\tau_{c,1} = -\frac{45\sqrt{3}}{32} \cdot \frac{\hbar}{\mu_B (A_{zz} - A_{xx}) \cdot (g_{zz} - \frac{1}{2}(g_{xx} + g_{yy}))} \cdot \frac{\Delta B_{0,pp}}{B_0} \cdot \left(\sqrt{\frac{h_0}{h_{-1}}} - \sqrt{\frac{h_0}{h_1}} \right) \quad (\text{S8})$$

$$\tau_{c,2} = \frac{9\sqrt{3}}{4\pi} \cdot \frac{\Delta B_{0,pp}}{(A_{zz} - A_{xx})^2} \cdot \left(\sqrt{\frac{h_0}{h_1}} + \sqrt{\frac{h_0}{h_{-1}}} - 2 \right) \quad (\text{S9})$$

whereas μ_B is the Bohr magneton, \hbar is the reduced Planck constant, B_0 is the center field in Tesla, $\Delta B_{0,pp}$ is the peak-to-peak linewidth of the central nitroxide resonance line ($m_l = 0$)

given in s^{-1} , and h_0 , h_{-1} and h_{+1} are the relative line heights of the three nuclear transitions ($m_l = -1, 0, +1$) in isotropic nitroxide spectra as shown in Figure S2b. The result from this analysis is given in Figure 2b (dark yellow). For convenience, error bars were not calculated for τ_c and are therefore assumed to range about 6% [S8].

S3 | Collective Lysine pK_a Estimation from pH-dependent EPR Experiments (5-MSL HSA)

The significant pH-dependence of the high-field (h_{-1}) and low-field (h_{+1}) peaks in CW EPR spectra from 5-MSL HSA (that are also used to calculate rotational correlation times τ_c in Supplementary Material S2) exhibit an odd maximum feature at about pH 10.4 (see Figure S3). Therefore, the results from PROPKA 3.0 calculations [S9–S11] on the fatty acid-free HSA structure (PDB ID: 1BM0) [S12] were tested for lysine pK_a values. Overall, $N_{Lys} = 58$ lysine residues have been considered in the charge calculation, apart from the Lys4 residue. Individual lysine $pK_{a,i}$ values ranged from 6.36 – 11.59 with an average:

$$pK_{a,Lys} = \frac{1}{N_{Lys}} \sum_{i=1}^{N_{Lys}} pK_{a,i} \quad (S10)$$

that yields $pK_{a,Lys} = 10.28 \pm 0.89$. This unexpected correspondence (Figure S3) may already facilitate the estimation of a collective lysine pK_a value ($pK_{a,Lys}$) from CW EPR spectra of 5-MSL HSA alone.

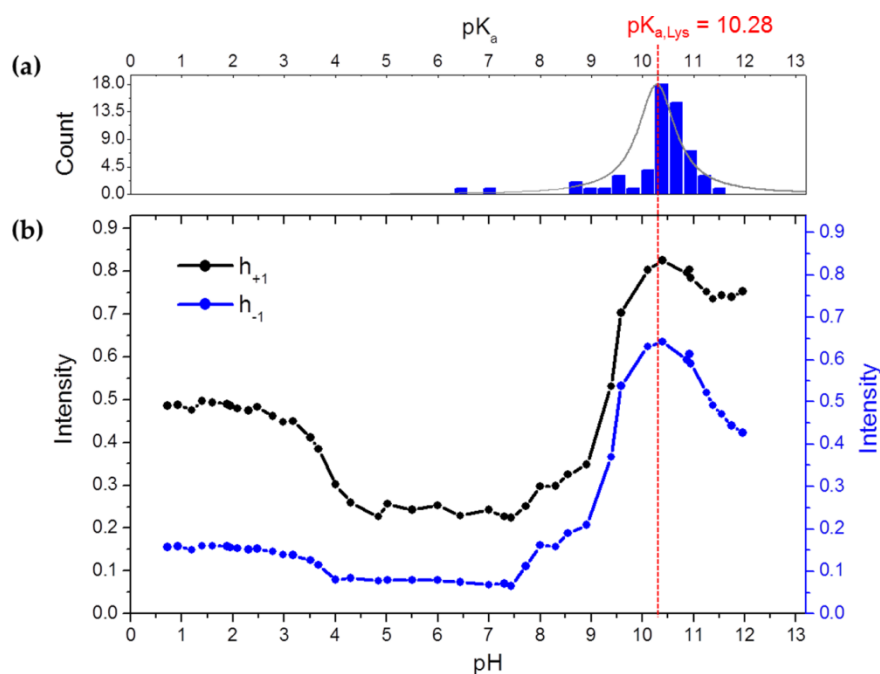


Figure S3. Correlation of lysine pK_a values and EPR spectral features of 5-MSL HSA. (a) Histogram of individual $pK_{a,i}$ values (blue) that were calculated with PROPKA 3.0 [S9–S11]. The histogram has been equipped with a Lorentz-distribution envelope curve (gray). (b) pH-dependent intensities of high-field (h_{-1} , blue) and low-field (h_{+1} , black) peaks are shown that appear in CW EPR spectra of 5-MSL HSA. The calculated average value $pK_{a,Lys}$ is highlighted as a red dotted line to indicate correspondence with EPR spectroscopic data.

S4 | Exemplary Simulation of 16-DSA Alone and Interacting with HSA

Two spectra were simulated with EasySpin [S13] according to a scheme that was presented earlier [S14]. Both spectra contain 16-DSA either in its free form (1:0 loading), or while interacting with HSA (2:1 loading, see Figure S4). The observed subspectra components $F_i(B)$ comprise 16-DSA in aggregates/micelles (a), free in solution (f), or bound to albumin (b_1, b_2) in the relative fractions ϕ_i .

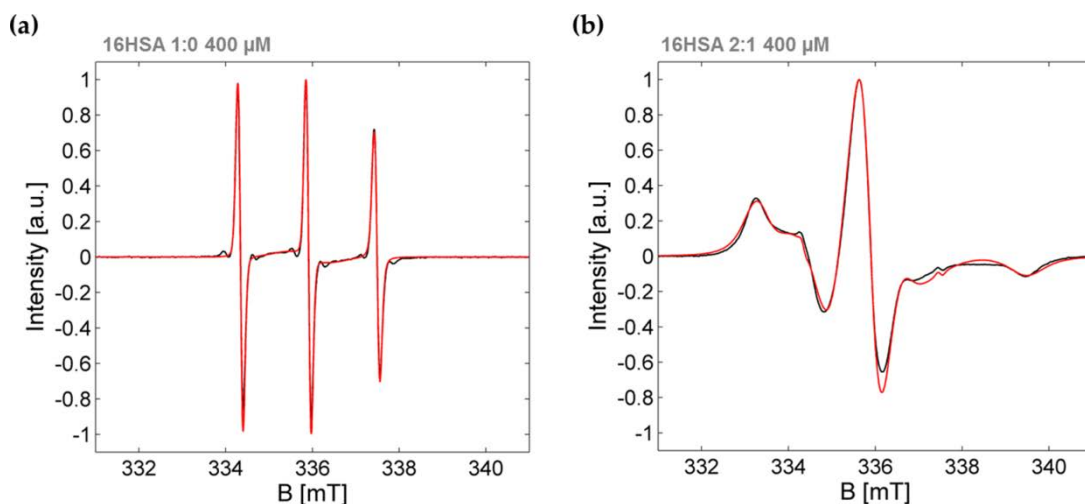


Figure S4. Exemplary spectral simulations from samples containing 16-DSA. Spectral simulations of (a) 0.4 mM 16-DSA-probed DPBS buffer with 20% v/v glycerol at pH 7.4 and (b) 16-DSA probed HSA in a 2:1 loading ratio (1 eq = 0.4 mM) in DPBS buffer at pH 7.4 and 20 % v/v glycerol. Experimental spectra are shown in black and simulations in red. For results of simulations see Table S1.

The obtained simulation parameters are listed in Table S1. In order to facilitate a comparison of the simulation parameters with extracted spectral features A_{\parallel} , A_{zz} and $\Delta B_{0,pp}$, all original values $A_{ii,sim}$ are multiplied with the sweep-field correction factor that was determined as $k_{SW} = 0.9923$ for all spin probe experiments, so that here $A_{ii} = A_{ii,sim} \cdot k_{SW}$.

Table S1. Simulation parameters from 16-DSA alone and 16-DSA-probed HSA

	$F_i(B)$	ϕ [%]	g_{xx}	g_{yy}	g_{zz}	A_{xx}^a [G]	A_{yy}^a [G]	A_{zz}^a [G]	a_{iso} [G]	τ_{cf} [ns]	β_i [°]
16HSA 1:0	f	63.42	2.0087	2.0064	2.0025	6.58	5.91	34.48	15.66	0.117	45
	a	36.58	2.0087	2.0064	2.0025	6.58	5.91	34.48	15.66	–	45
16HSA 2:1	f	0.07	2.0087	2.0064	2.0025	6.58	5.91	34.48	15.66	0.117	45
	b_1	62.08	2.0089	2.0064	2.0025	5.91	5.42	34.34	15.22	14.232	16
	b_2	37.85	2.0089	2.0064	2.0025	5.91	5.42	34.34	15.22	5.837	45

^aValues were corrected with $k_{SW} = 0.9923$ as simulations were conducted on experimental spectra.

Exemplary subspectra $F_i(B)$ were calculated according to values given in Table S1 and are presented in Figure 3d. 16-DSA probes emerging in aggregates (a) were simulated with an effective Heisenberg spin exchange frequency $J_{AB} = 45$ MHz.

S5 | Rationalization and Analyses of I_{abf} curves

All I_{abf} values were calculated according to equation 1 and corresponding errors were therefore obtained with:

$$\Delta I_{abf} = \left| \frac{\Delta h_{\perp} + \Delta h_{-1}}{h_0} \right| + \left| \frac{h_{\perp} \Delta h_0}{h_0^2} \right| \quad (S11)$$

The different transition zones of 16-DSA-probed HSA in I_{abf} curves were extrapolated by fit curves for a better extraction of decisive pH values. The curve shape reproduction for pH regions from pH 1 – 4 (16-DSA micellation ($j = a$)) and pH 4 – 9 (slight changes in h_{\perp} ($j = b$)) is facilitated best with the use of Boltzmann functions of the kind:

$$I_{abf} = I_{j,\max} + \frac{(I_{j,\max} - I_{j,\min})}{1 + e^{(\text{pH} - \text{pH}_{j,0})/\text{dpH}_j}} \quad (S12)$$

This allows for an estimation of individual transition heights $I_j = I_{j,\max} - I_{j,\min}$, transition midpoints $\text{pH}_{j,0}$ and corresponding widths dpH_j . The resulting fit curves are presented in Figure S5a–d and the fit parameters can be found in Table S2.

Table S2. Boltzmann fit parameters obtained from I_{abf} curves (16-DSA)

Parameter	16HSA 1:1		16HSA 2:1	
	a	b	a	b
pH fit range	0.98 – 4.39	3.94 – 8.51	0.89 – 4.79	3.99 – 10.27
$I_{j,\max}$	0.0742 ± 0.0049	-0.1754 ± 0.0119	0.2424 ± 0.0098	-0.1999 ± 0.0015
$I_{j,\min}$	-0.1732 ± 0.0043	-0.0724 ± 0.0055	-0.2004 ± 0.0032	-0.0895 ± 0.0008
$\text{pH}_{j,0}$	3.436 ± 0.026	5.600 ± 0.214	3.445 ± 0.028	6.188 ± 0.033
dpH_j	0.189 ± 0.021	0.665 ± 0.195	0.158 ± 0.015	0.564 ± 0.028
R^2	0.9939	0.9751	0.9932	0.9976

The relative amount of free ligand can be observed in Figure 4d by monitoring the ratio h_{-1}/h_0 . The emergence of the bump feature from pH 4.5 to about pH 8.5 indicates a clear increase in the amount of free ligand. The bump can be described by a conventional Gaussian curve shape of the form:

$$\frac{h_{-1}}{h_0} = I_{f,0} + I_f \cdot e^{-\frac{1}{2} \left(\frac{\text{pH} - \text{pH}_{f,0}}{\sigma_{f,0}} \right)^2} \quad (S13)$$

and the fit curves are given in Figure S5e and S5f. Obviously the inflection point $\text{pH}_{a,0}$ is at pH 3.45 and the maximum at $\text{pH}_{f,0}$ is located around pH 6.2 for both 16-DSA loading ratios.

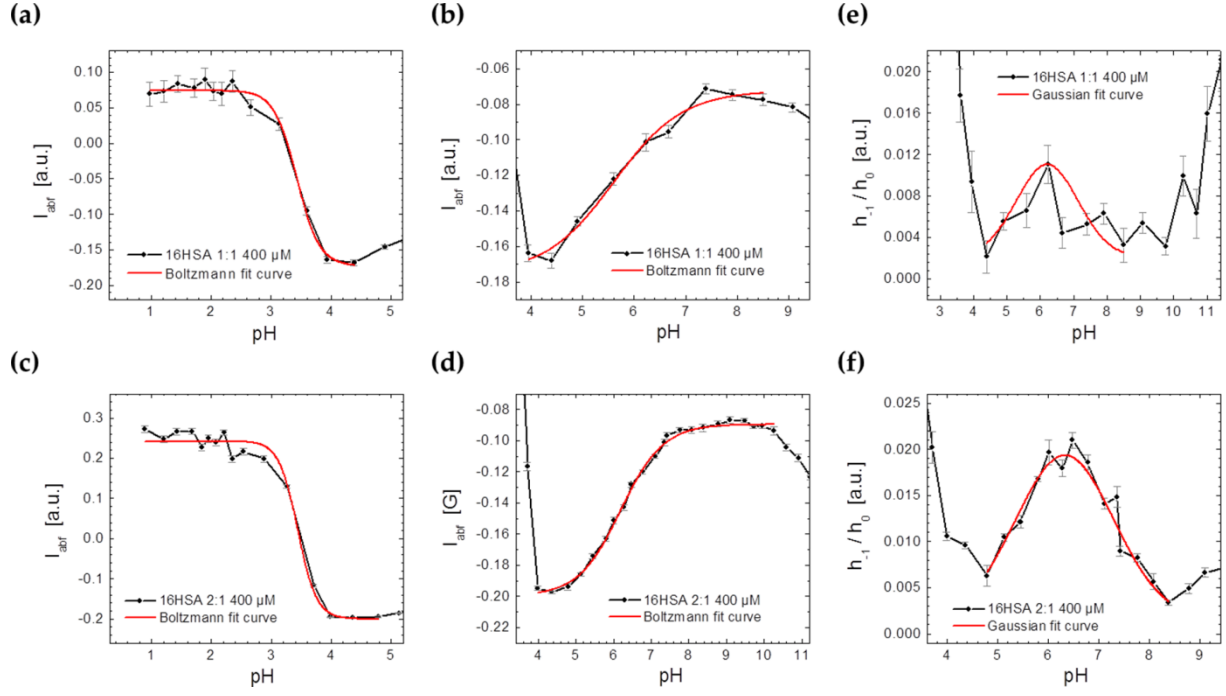


Figure S5. Fit curves from pH-dependent I_{abf} and h_{-1}/h_0 parameters. Boltzmann fit curves (equation S12) to I_{abf} for 16-DSA-probed HSA (1:1 loading ratio) (a) in the acidic (pH 1 – 4) and (b) in the neutral pH range (pH 4 – 9). Boltzmann fit curves to I_{abf} for 16-DSA-probed HSA (2:1 loading) (c) in the acidic (pH 1 – 4) and (d) in the neutral pH range (pH 4 – 9). Gaussian fit curves (equation S13) to the relative high field peak heights h_{-1}/h_0 for 16-DSA-probed HSA are given in the range from pH 4.5 – 8.5 for (e) 1:1 and (f) 2:1 loading. Results are shown in Table S2 and Table S3.

Table S3. Gaussian fit parameters obtained from h_{-1}/h_0 curves (16-DSA)

Parameter	1:1	2:1
pH fit range	4.39 – 8.51	4.79 – 8.38
$I_{f,0}$	0.0021	0.0016 ± 0.0012
$\text{pH}_{f,0}$	6.204 ± 0.209	6.327 ± 0.037
$\sigma_{f,0}$	0.929 ± 0.155	0.972 ± 0.091
I_f	0.00891	0.01775 ± 0.00114
FWHM	2.187	2.288
Area	0.0207	0.0432
R^2	0.6601	0.9709

The curve shape for minima in I_{abf} that occur around $\text{pH}_a \approx 4$ and $\text{pH}_f \approx 11$ is of a more intricate mathematical nature. Here, a rational Nelder model function [S15] is used that facilitates the reproduction of data sets containing asymmetric extrema. The applied function:

$$I_{abf} = \frac{\text{pH} + \alpha}{\beta_0 + \beta_1(\text{pH} + \alpha) + \beta_2(\text{pH} + \alpha)^2} \quad (\text{S14})$$

allows for this circumstance here.

Table S4. Nelder fit parameters obtained from I_{abf} curves (16-DSA)

Parameter	1:1		2:1	
pH fit range	3.14 – 6.67	9.08 – 12.38	3.26 – 6.28	9.96 – 12.24
α	-3.241 ± 0.032	-12.074 ± 0.011	-3.418 ± 0.026	-12.102 ± 0.018
β_0	-3.118 ± 0.452	1.707 ± 0.071	-1.458 ± 0.165	1.823 ± 0.175
β_1	0.169 ± 0.743	-1.927 ± 0.196	-1.957 ± 0.375	-1.674 ± 0.807
β_2	-3.002 ± 0.285	3.394 ± 0.167	-1.541 ± 0.182	4.463 ± 0.723
R^2	0.9770	0.9937	0.9630	0.9666

In order to detect these extrema from the curve fits, a general derivation according to the quotient rule gives:

$$\frac{\partial I_{abf}}{\partial \text{pH}} = \frac{1}{\beta_0 + \beta_1(\text{pH} + \alpha) + \beta_2(\text{pH} + \alpha)^2} - \frac{(\text{pH} + \alpha) \cdot (2\beta_2(\text{pH} + \alpha) + \beta_1)}{(\beta_0 + \beta_1(\text{pH} + \alpha) + \beta_2(\text{pH} + \alpha)^2)^2} = 0 \quad (\text{S15})$$

Obtaining the zeros of this function is straightforward and reveals that:

$$\text{pH}_{\min} = -\alpha \pm \sqrt{\frac{\beta_0}{\beta_2}} \quad (\text{S16})$$

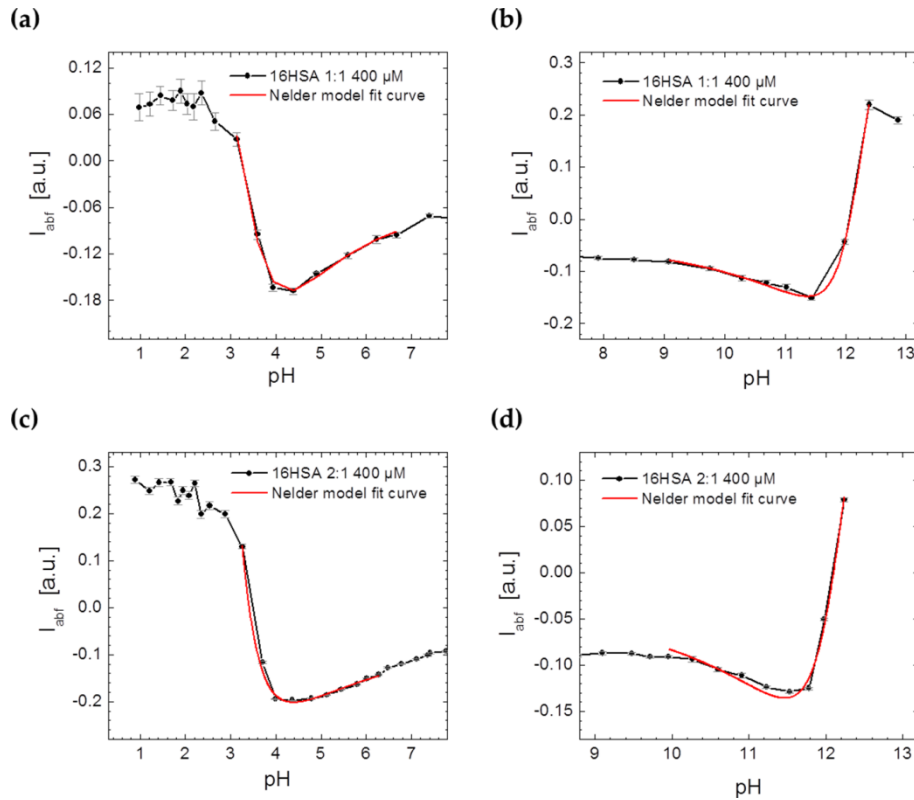


Figure S6. Nelder fit curves from pH-dependent I_{abf} values. Nelder fit curves (equation S14) to I_{abf} for 16-DSA-probed HSA (1:1 loading) (a) in the acidic (pH 3 – 6) and (b) in the basic pH range (pH 9 – 12). Nelder fit curves to I_{abf} for 16-DSA-probed HSA (2:1 loading) (c) in the acidic (pH 3 – 6) and (d) in the basic pH range (pH 9 – 12). Results ($R^2 > 0.962$) from the curve regressions are given in Table S4.

with the errors:

$$\Delta\text{pH}_{\min} = \frac{\Delta\beta_0}{2\beta_2\sqrt{\frac{\beta_0}{\beta_2}}} + \frac{\beta_0\Delta\beta_2}{2\beta_2^2\sqrt{\frac{\beta_0}{\beta_2}}} + \Delta\alpha \quad (\text{S17})$$

Therefore, the β_1 parameter is obviously of inferior importance. It is also found that the sign in equation S16 depends on the curve symmetry, so that the acidic minimum is located at $\text{pH}_a = -\alpha + (\beta_0/\beta_2)^{-1/2}$ and the basic minimum $\text{pH}_f = -\alpha - (\beta_0/\beta_2)^{-1/2}$. The corresponding fit curves are given in Figure S6.

S6 | Analysis of pH-dependent Apparent Hyperfine Coupling Constants A_{\parallel}

The obtained curves for A_{\parallel} values (Figure 5b) in the region around pH 2 were fitted with Gaussian functions:

$$A_{\parallel} = A_{\parallel,0} + I_{A,\text{MG}} \cdot e^{-\frac{1}{2}z^2} \quad (\text{S18})$$

with

$$z = (\text{pH} - \text{pH}_{\text{MG}})/\sigma_{\text{MG}} \quad (\text{S19})$$

for 5-DNA-probed HSA (2:1 loading).

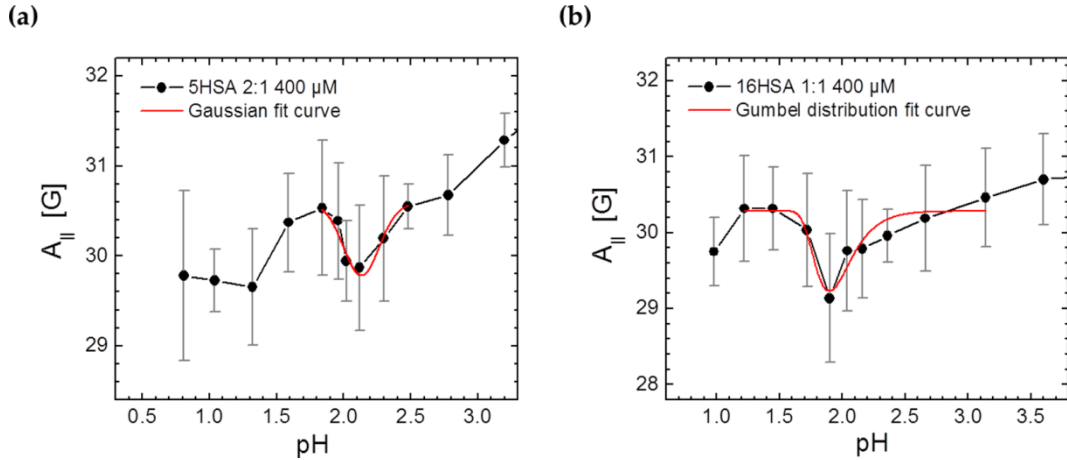


Figure S7. Fit curves of pH-dependent A_{\parallel} values in the range from pH 1 – 3. A Gaussian fit curve was applied to reproduce (a) A_{\parallel} values from 5-DNA-probed HSA (2:1 loading) in the acidic range from pH 1.8 – 2.5 and a Gumbel distribution [S16] was used to reproduce (b) A_{\parallel} values from 16-DNA-probed HSA (1:1 loading) in the acidic range from pH 1.2 – 3.1. Results are shown in Table S5.

For 16-DNA-probed HSA (1:1 loading) an extreme value distribution function was adopted according to Gumbel [S16]:

$$A_{\parallel} = A_{\parallel,0} + I_{A,\text{MG}} \cdot e^{(e^{-z} - z + 1)} \quad (\text{S20})$$

Here, $A_{||,0}$ is the ambient value around the indentation around pH 2.0 and $I_{A,MG}$ is the fitted indentation depth of a corresponding feature.

Table S5. Gaussian Fit parameters obtained from $A_{||}$ curves

Parameter	5HSA 2:1	16HSA 1:1
Fit range	1.84 – 2.48	1.22 – 3.14
Model	Gauss (eq. S18)	Gumbel (eq. S20)
$A_{ ,0}$	30.583 ± 0.089	30.284 ± 0.086
pH_{MG}	2.133 ± 0.026	1.898 ± 0.029
σ_{MG}	0.133 ± 0.037	0.142 ± 0.028
$I_{A,MG}$	-0.802 ± 0.016	-1.054 ± 0.183
FWHM	0.3128	–
R^2	0.8730	0.8119

S7 | Determination of Low Temperature A_{zz} Values at $T = 150$ K from Spin Probed HSA

The g_{xx} and A_{zz} tensor values are the most sensitive quantities when changes in polarity are to be detected [S17]. In a straightforward procedure, outer extrema separations of spectra at $T = 150$ K were used as it was already shown in Supplementary Material S2. $A_{zz,k}$ from spin probes k are here observed as a function of pH and the corresponding individual experimental findings are summarized in Figure S8 and Table S6. Individual values of $A_{zz,k}$ and their uncertainties have been obtained by using equation S2 and S3.

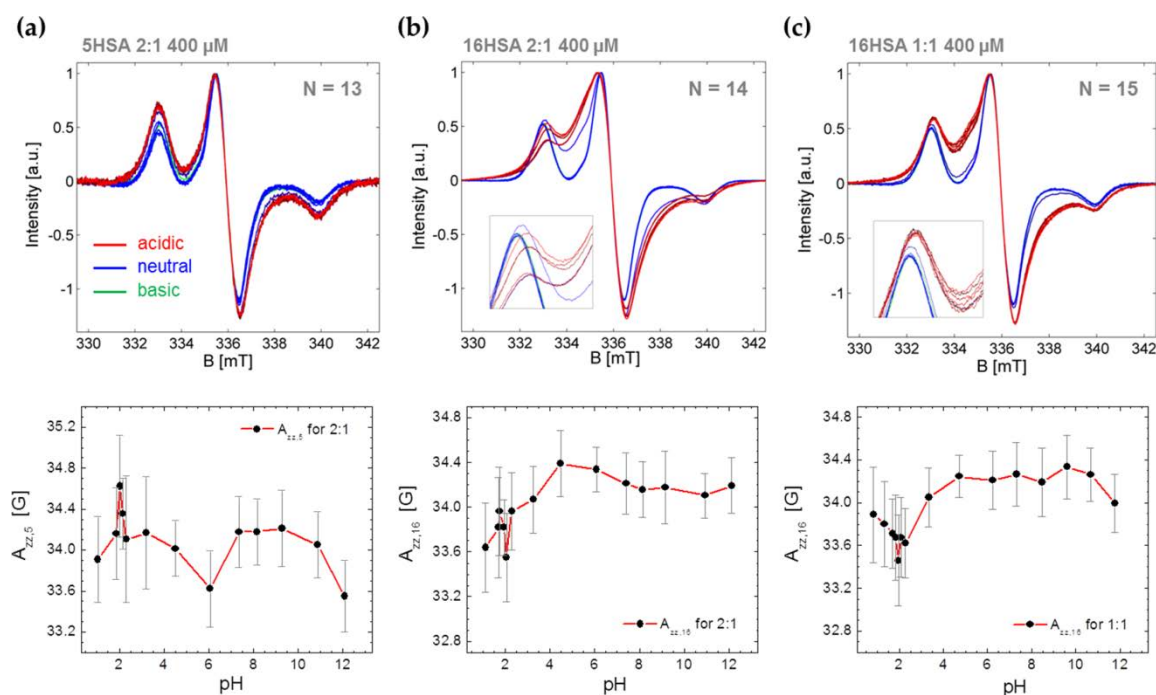


Figure S8. A_{zz} parameters from low temperature CW EPR spectra at $T = 150$ K. Here, color coded experimental spectra are presented in terms of the pH region of interest. The acidic range is shown in red ($\text{pH} < 4$), the neutral range in blue ($4 < \text{pH} < 11$) and the basic range is shown in green ($\text{pH} > 11$). CW EPR spectra (top) are given together with the extracted $A_{zz,k}$ values (bottom) for (a) 5-DSA-probed HSA (2:1 loading, $N = 13$), (b) 16-DSA-probed HSA (2:1 loading, $N = 14$) and (c) with 1:1 loading ($N = 15$). Inset graphs are given for 16-DSA-probed HSA samples and highlight regions where strong spectral changes appear.

Table S6. A_{zz} values from spin probed HSA as a function of pH^a

5HSA 2:1		16HSA 2:1		16HSA 1:1			
pH	$A_{zz,5}$ [G]	pH	$A_{zz,16}$ [G]	pH	$A_{zz,16}$ [G]	pH ^b	δA_{zz} ^c [G]
1.04	33.91 ± 0.42	1.13	33.64 ± 0.40	0.83	33.89 ± 0.45	1.09 ± 0.06	0.27 ± 0.41
1.87	34.16 ± 0.45	1.71	33.82 ± 0.45	1.33	33.80 ± 0.40	1.79 ± 0.11	0.34 ± 0.45
2.03	34.62 ± 0.50	1.75	33.96 ± 0.40	1.70	33.71 ± 0.32	2.05 ± 0.02	1.07 ± 0.45
2.16	34.35 ± 0.35	1.96	33.82 ± 0.25	1.85	33.68 ± 0.40	2.31 ± 0.01	0.14 ± 0.48
2.31	34.10 ± 0.62	2.06	33.55 ± 0.40	1.97	33.46 ± 0.42	3.23 ± 0.04	0.10 ± 0.42
3.20	34.17 ± 0.55	2.30	33.96 ± 0.35	2.08	33.68 ± 0.37	4.50 ± 0.02	-0.38 ± 0.29
4.51	34.02 ± 0.27	3.26	34.07 ± 0.30	2.28	33.62 ± 0.32	6.08 ± 0.01	-0.71 ± 0.29
6.07	33.62 ± 0.37	4.48	34.39 ± 0.30	3.35	34.05 ± 0.27	7.39 ± 0.04	-0.04 ± 0.31
7.36	34.18 ± 0.35	6.08	34.34 ± 0.20	4.72	34.25 ± 0.20	8.16 ± 0.01	0.02 ± 0.29
8.17	34.18 ± 0.32	7.41	34.21 ± 0.27	6.24	34.21 ± 0.27	9.22 ± 0.09	0.04 ± 0.35
9.28	34.21 ± 0.37	8.15	34.16 ± 0.25	7.32	34.27 ± 0.30	10.90 ± 0.04	-0.05 ± 0.26
10.87	34.05 ± 0.32	9.15	34.18 ± 0.32	8.48	34.19 ± 0.32	12.11 ± 0.02	-0.64 ± 0.30
12.09	33.55 ± 0.35	10.93	34.10 ± 0.20	9.61	34.34 ± 0.30		
-	-	12.12	34.19 ± 0.25	10.68	34.27 ± 0.25		
-	-	-	-	11.78	34.00 ± 0.27		
$A_{zz,k,pH}$ ^d [G]	34.09 ± 0.28		34.03 ± 0.25		33.96 ± 0.29		

^aValues are taken from spectra in Figure S8. ^b5-DSA and 16-DSA experiments with 2:1 loading and approximate overlapping pH values are summarized by an average pH value together with its mean deviation. ^c δA_{zz} values are given together with an averaged error from $A_{zz,5}$ and $A_{zz,16}$ (see equation S21 and Figure 5c). ^d $A_{zz,k,pH}$ = averaged $A_{zz,k}$ values across all pH are given with their standard deviation.

Differences in between $A_{zz,5}$ and $A_{zz,16}$ in the 2:1 loading status are detected by the differences at similar or identical pH values with:

$$\delta A_{zz} = A_{zz,5} - A_{zz,16} \quad (\text{S21})$$

and are listed on the right hand side of Table S6. Additionally, a pH-independent average value is given by $A_{zz,k,pH}$ in the bottom line.

S8 | Analysis of $\Delta B_{0,pp}$ Curves

The obtained curve sections for $\Delta B_{0,pp}$ in Figure 6b were fitted with Gaussian functions of the kind:

$$\Delta B_{0,pp} = \Delta B_{0,pp,\min,j} + \Delta B_{0,pp,\max,j} \cdot e^{-\frac{1}{2} \left(\frac{\text{pH} - \text{pH}_j}{\sigma_j} \right)^2} \quad (\text{S22})$$

in the range from about pH 0.9 – 3.3 ($j = \text{MG}$) for all spin probes and additionally from pH 3.9 – 8.5 for 5-DSA ($j = \text{B},0$). The obtained fit parameters are given in Table S7. The resulting Gauss fit curves are shown in Figure S9a–d.

Table S7. Gaussian fit parameters obtained from $\Delta B_{0,pp}$ curves

Parameter	5HSA 2:1		16HSA 2:1	16HSA 1:1
j	MG	B,0	MG	MG
pH fit range	1.76 – 2.78	3.87 – 8.52	0.89 – 3.26	1.22 – 2.66
$\Delta B_{0,pp,min,j}$	–	7.829	–	4.222 ± 0.007
pH $_j$	2.164 ± 0.024	6.245 ± 0.076	1.866 ± 0.072	2.007 ± 0.010
σ_j	0.369 ± 0.032	0.954 ± 0.081	0.948 ± 0.496	0.127 ± 0.012
$\Delta B_{0,pp,max,j}$	–	-0.755 ± 0.054	–	-0.196 ± 0.013
FWHM	0.868	2.246	2.233	0.298
R ²	0.8997	0.8897	0.8198	0.9714

The transition region from about pH 3 – 9 for 16-DSA was reproduced best with the use of Boltzmann functions of the kind:

$$\Delta B_{0,pp} = \Delta B_{0,pp,max} + \frac{(\Delta B_{0,pp,min} - \Delta B_{0,pp,max})}{1 + e^{(\text{pH} - \text{pH}_{B,0})/\text{dpH}_{B,0}}} \quad (\text{S23})$$

This allows for an estimation of the transition height $I_{B,j} = \Delta B_{0,pp,max} - \Delta B_{0,pp,min}$, the transition midpoint $\text{pH}_{B,0}$ and its corresponding width $\text{dpH}_{B,0}$. The fit curves are presented in Figure S9e and S9f with the respective parameters shown in Table S8.

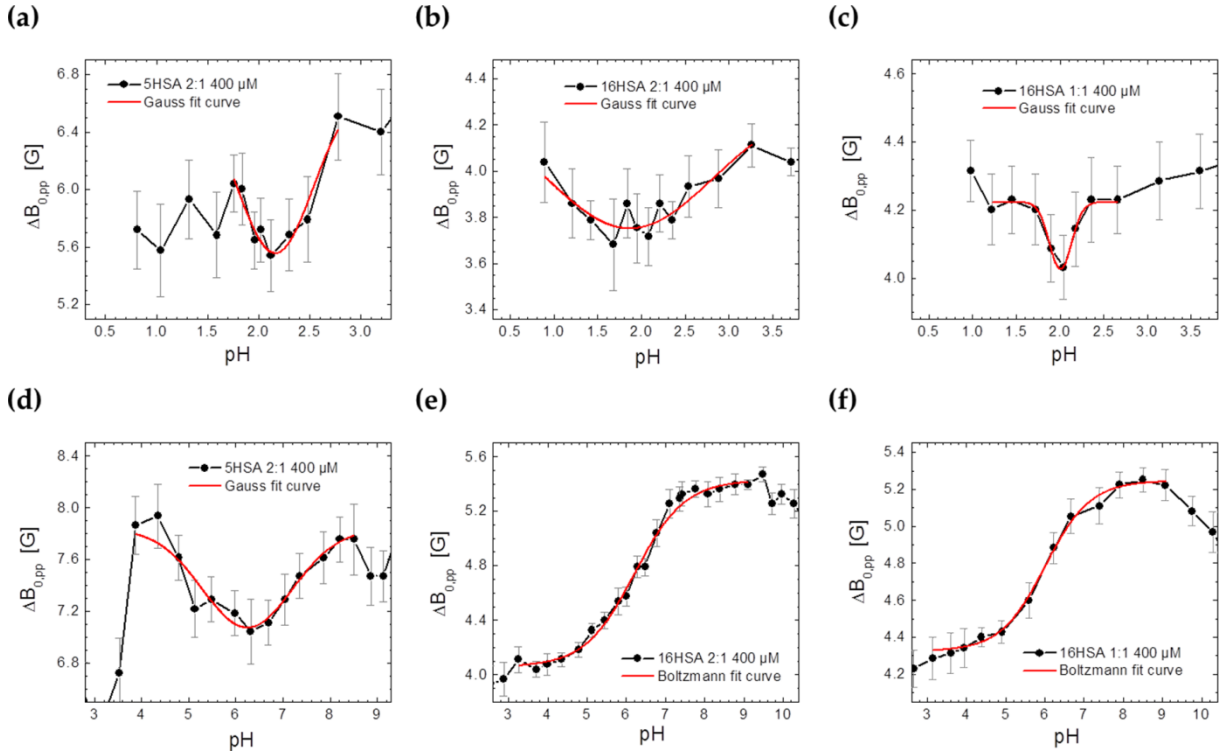


Figure S9. Fit curves from $\Delta B_{0,pp}$. Gaussian fit curves were applied to reproduce $\Delta B_{0,pp}$ values from (a) 5-DSA-probed HSA (2:1 loading) in the acidic range from pH 1.8 – 2.8, (b) 16-DSA-probed HSA (2:1) in the acidic range from pH 0.9 – 3.3, (c) 16-DSA-probed HSA (1:1) in the acidic range from pH 1.2 – 2.7 and (d) 5-DSA-probed HSA (2:1) in the neutral range from pH 3.9 – 8.5. All corresponding parameters are given in Table S7. Boltzmann fit curves were applied to reproduce $\Delta B_{0,pp}$ values from (e) 16-DSA-probed HSA (2:1) in the neutral range from pH 3.3 – 9.1 and (f) 16-DSA-probed HSA (1:1) in the neutral range from pH 3.1 – 9.1 with a complete set of parameters given in Table S8.

Table S8. Boltzmann fit parameters obtained from $\Delta B_{0,pp}$ curves (16-DSA)

Parameter	16HSA 2:1	16HSA 1:1
Fit range	3.26 – 9.10	3.14 – 9.08
$\Delta B_{0,pp,min}$	4.055 ± 0.033	4.323 ± 0.025
$\Delta B_{0,pp,max}$	5.428 ± 0.025	5.246 ± 0.020
pH _{B,0}	6.209 ± 0.060	6.008 ± 0.074
dpH _{B,0}	0.634 ± 0.059	0.573 ± 0.070
R ²	0.9929	0.9945

S9 | Further Information about Order Parameters S and Wobbling Angles γ

The setup of an order parameter S (see equation 3, Figure 7) for HSA requires knowledge about the “crystalline” hyperfine coupling tensor values (A_{ii}) that can be extracted from spectral simulations of the bound ligand subspectra (b_1 and b_2 , see Table S1). It is here insufficient to only use the low temperature A_{zz} values given in Table S6. However, experimental ($A_{zz,16,exp} = 34.21$ G, pH 7.40) values compare well to the simulated ones ($A_{zz,16,sim} = 34.34$ G, pH 7.41) of bound fatty acids at physiological pH. With these simulations the denominator expression ($A_{zz} - A_{xx}$) = 28.43 G in equation 3 becomes accessible. For simplicity it is kept constant at all pH values as the relative changes in the expression ($A_{zz} - A_{xx}$) for bound fatty acids with pH can be considered as small (well below 6%). The errors for pH-dependent order parameters S were determined by propagation of uncertainty:

$$\Delta S = \left| \frac{\partial S}{\partial x} \right| \Delta x = \left(\frac{a_{iso,b}}{a_{iso,S}} \cdot \frac{1}{(A_{zz} - A_{xx})} \right) \cdot (\Delta A_{\parallel} + \Delta A_{\perp}) + \left(\frac{a_{iso,b}}{a_{iso,S}} \cdot \frac{(A_{\parallel} - A_{\perp})}{(A_{zz} - A_{xx})^2} \right) \cdot (\Delta A_{zz} + \Delta A_{xx}) + \left(\frac{1}{a_{iso,S}} \cdot \frac{(A_{\parallel} - A_{\perp})}{(A_{zz} - A_{xx})} \right) \cdot \left(\Delta a_{iso,b} + \frac{a_{iso,b}}{a_{iso,S}} \cdot \Delta a_{iso,S} \right) \quad (S24)$$

with $\Delta A_{ii} = \Delta a_{iso,b} = 0.1$ G, $\Delta a_{iso,b} = 0.14 - 0.53$ G, $\Delta A_{\parallel} = 0.12 - 0.94$ G and $\Delta A_{\perp} = 0.12 - 0.57$ G. The derivation of equation 4b is facilitated straightforward from equation 4a. Thus, substitution of $\cos\gamma$ with x leads to the quadratic expression:

$$2S = \cos\gamma + \cos^2\gamma = x + x^2 \quad (S25)$$

that yields:

$$x_1 = \frac{\sqrt{8S+1}-1}{2} = \cos\gamma_1 = \cos\gamma \quad (S26)$$

and therefore:

$$\gamma = \arccos\left(\frac{\sqrt{8S+1}-1}{2}\right) \quad (S27)$$

From equation S27 the error $\Delta\gamma$ of the wobbling angle is obtained as:

$$\Delta\gamma = \left| \frac{\partial\gamma}{\partial S} \right| \Delta S = \left| -\frac{2}{\sqrt{8S+1} \cdot \sqrt{1 - \left(\frac{\sqrt{8S+1}-1}{2}\right)^2}} \right| \cdot \Delta S \quad (\text{S28})$$

Again, the region from pH 1.2 – 3.6 can be fitted best with appropriate Gaussian functions, both for the order parameter (Figure S10):

$$S = S_0 + I_{S,\text{MG}} \cdot e^{-\frac{1}{2}z^2} \quad (\text{S29})$$

as well as for the wobbling angle:

$$\gamma = \gamma_0 + I_{\gamma,\text{MG}} \cdot e^{-\frac{1}{2}z^2} \quad (\text{S30})$$

The parameter z corresponds to the expression in equation S19 and the corresponding fit parameters are given in Table S9.

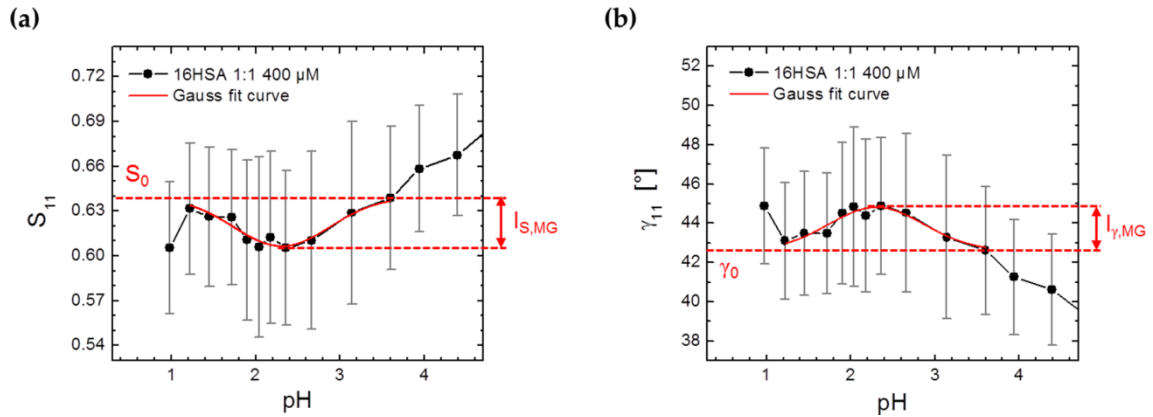


Figure S10. Fit curves from pH-dependent order parameters S and wobbling angles γ . Gaussian fit curves were applied to the pH region from 1.2 – 3.6 of 16-DNA-probed HSA (1:1) in order to reproduce values from (a) order parameter S and (b) wobbling angle γ best. Here, the indentation depths $I_{S,\text{MG}}$ and $I_{\gamma,\text{MG}}$ are highlighted in red.

Table S9. Gaussian fit parameters from order parameter (S) and wobbling angle (γ) curves

Parameter	16HSA 1:1	Parameter	16HSA 1:1
Fit range	1.22 – 3.60	Fit range	1.22 – 3.60
S_0	0.639 ± 0.007	γ_0	42.596 ± 0.452
pH_{MG}	2.308 ± 0.068	pH_{MG}	2.307 ± 0.068
σ_{MG}	0.566 ± 0.151	σ_{MG}	0.569 ± 0.152
$I_{S,\text{MG}}$	-0.0325 ± 0.0062	$I_{\gamma,\text{MG}}$	2.209 ± 0.427
FWHM	1.334	FWHM	1.340
R^2	0.8685	R^2	0.8687

S10 | Shift of $P_{\max}(r)$ in DEER Data from pH Denaturation of 16-DSA Spin Probed HSA

The assessment of background dimensionalities in DEER spectroscopy is a delicate subject and is here only given as a qualitative estimate in Figure S11. However, the pH-dependent peak shift of $P_{\max}(r)$ is clearly detectable in Figure 8e and 8f and is depicted in Figure 9a. The corresponding curve shape was reconstructed by a Boltzmann type function in Origin that yields values presented in Table S10 for equation 5 in the main text.

Table S10. Fit parameters from equation 5 in the main text

Parameter	16HSA 2:1
r_{\min}	3.455 ± 0.008
r_{\max}	3.964 ± 0.024
$\text{pH}_{P,0}$	6.161 ± 0.130
$\text{dpH}_{P,0}$	1.156 ± 0.108
R^2	0.9972

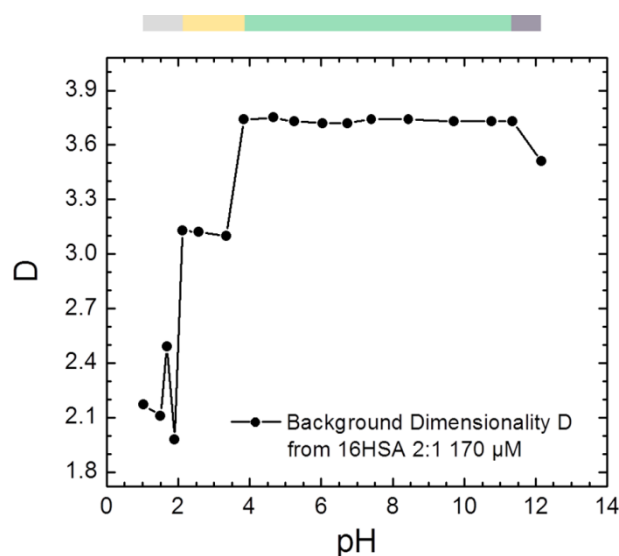


Figure S11. DEER background of 16-DSA-probed HSA as a function of pH (2:1 loading). Background dimensionalities D from DEER time traces of 0.17 mM HSA in Figure 8 are shown as a function of pH. The corresponding extended (E), fast migrating (F), compact (C) and aged (A) conformers are given in the phase space bar (top lane).

S11 | Functional Phase Space of HSA as Obtained from EPR Spectroscopy (and DLS)

The construction of Figure 11 was facilitated by a combined set of pH ranges that were obtained from different parameters from CW EPR (5-MSL HSA, 5-DSA- and 16-DSA-probed HSA), DEER (16-DSA) and DLS experiments that are summarized in Table S11.

Table S11 | Functional phase onsets of HSA from pH-dependent EPR and DLS experiments^a

Method	Reporter	Data	MG	F	pH _{α,0}	C or N	pH _α	pI	S _{max}	B	pH _{opt}	A	pH _f	
CW EPR	5-MSL	<i>A</i>	–	2.78	–	3.67	–	–	–	–	–	> 10.87	–	
		<i>τ</i> _c	–	2.78	–	4.01	–	–	–	7.44	9.58	(> 9.58)	–	
	5-DSA (2:1)	<i>A</i>	2.13	2.78	–	3.87	–	–	–	–	7.86	9.84	(> 9.84)	–
		<i>A</i> _{zz}	2.03	–	–	–	–	–	–	–	–	–	–	–
		$\Delta B_{0,pp}$	2.16	2.78	–	3.87	–	6.25	–	–	8.21	9.43	> 11.19	–
	16-DSA (2:1)	<i>A</i>	–	3.26	–	4.79	–	–	–	–	–	–	> 11.23	–
		<i>A</i> _{zz}	2.06	–	–	–	–	–	–	–	–	–	–	–
		$\Delta B_{0,pp}$	1.87	3.26	–	–	–	6.21	–	–	(7.11)	(9.48)	(> 9.48)	–
		<i>I</i> _{abf}	–	–	3.45	–	4.39	6.19	–	–	–	–	–	11.46
		<i>h</i> ₋₁ / <i>h</i> ₀	–	–	–	–	–	6.33	–	–	–	–	–	–
		<i>S</i> / <i>γ</i>	–	–	–	–	–	–	–	7.76	–	–	–	–
	16-DSA (1:1)	<i>A</i>	1.90	2.66	–	3.60	–	–	–	–	–	–	> 11.02	–
		<i>A</i> _{zz}	1.97	–	–	–	–	–	–	–	–	–	–	–
		$\Delta B_{0,pp}$	2.01	3.14	–	–	–	6.01	–	–	(6.67)	(9.76)	> 11.02	–
		<i>I</i> _{abf}	–	–	3.44	–	4.26	5.60	–	–	–	–	–	11.36
		<i>h</i> ₋₁ / <i>h</i> ₀	–	–	–	–	–	6.20	–	–	–	–	–	–
		<i>S</i> / <i>γ</i>	2.31	–	–	–	–	–	–	7.40	–	–	–	–
	DEER	16-DSA (2:1)	Δ	–	2.57	–	3.83	–	–	–	–	–	> 11.35	–
			<i>D</i>	–	2.12	–	3.83	–	–	–	–	–	–	≥ 11.35
<i>r</i>			–	–	–	3.83	–	6.16	–	–	–	–	≥ 11.35	–
DLS	–	<i>R</i> _H	–	3.53	–	4.29	–	–	–	–	–	≥ 11.70	–	
		(A.M.)	2.05	2.88	3.45	3.96	4.33	6.12	7.58	7.84	9.62	11.23	11.41	
		(S.D.)	0.14	0.39	0.01	0.35	0.09	0.23	0.21	0.39	0.21	0.25	0.07	

^aValues in parentheses are either experimental singularities or were not used for calculations of an arithmetic mean (A.M.) or a standard deviation (S.D.). Values from PROPKA calculations (Figure 1) and ANS fluorescence (Figure 2d) were not considered in this list.

An averaged value was determined across all experiments that contain reasonable peculiarities (values without parentheses). The E form is assumed to occur at pH values below the onset of the F form (\leq pH 2.9) and comprises the emergence of the molten globule (MG) state. Therefore an E form is not explicitly mentioned. The compact form (C) reaches from the onset of the N form to the onset of the A form and can be subdivided in three compartments, the N₁, B and N₂ form.

S12 | Supplementary References

- S1. Hubbell, W.L.; McConnell, H.M. Molecular Motion in Spin-Labeled Phospholipids and Membranes. *J. Am. Chem. Soc.* **1971**, *93*, 314–326.
- S2. Meirovitch, E.; Freed, J.H. Analysis of Slow-Motional Electron Spin Resonance Spectra in Smectic Phases in Terms of Molecular Configuration, Intermolecular Interactions, and Dynamics. *J. Phys. Chem.* **1984**, *88*, 4995–5004.
- S3. Steinhoff, H.J.; Lieutenant, K.; Schlitter, J. Residual Motion of Hemoglobin-Bound Spin Labels as a Probe for Protein Dynamics. *Z. Naturforsch. C* **1989**, *44*, 280–288.
- S4. Stone, T.J.; Buckman, T.; Nordio, P.L.; McConnell, H.M. Spin-Labeled Biomolecules. *Proc. Natl. Acad. Sci. USA* **1965**, *54*, 1010–1017.
- S5. Waggoner, A.S.; Griffith, O.H.; Christensen, C.R. Magnetic Resonance of Nitroxide Probes in Micelle-Containing Solutions. *Proc. Natl. Acad. Sci. USA* **1967**, *57*, 1198–1205.
- S6. Marzola, P.; Pinzino, C.; Veracini, C.A. Spin-Labeling Study of Human Serum Albumin in Reverse Micelles. *Langmuir* **1991**, *7*, 238–242.
- S7. Bulla, I.; Törmälä, P.; Lindberg, J.J. Spin Probe Studies on the Dynamic Structure of Dimethyl Sulfoxide-Water Mixtures. *Acta Chem. Scand. Ser. A* **1975**, *29*, 89–92.
- S8. Strancar, J.; Koklic, T.; Arsov, Z.; Filipic, B.; Stopar, D.; Hemminga, M.A. Spin Label EPR-Based Characterization of Biosystem Complexity. *J. Chem. Inf. Model.* **2005**, *45*, 394–406.
- S9. Li, H.; Robertson, A.D.; Jensen, J.H. Very Fast Empirical Prediction and Rationalization of Protein pK_a Values. *Proteins Struct. Funct. Bioinf.* **2005**, *61*, 704–721.
- S10. Bas, D.C.; Rogers, D.M.; Jensen, J.H. Very fast prediction and rationalization of pK_a values for protein-ligand complexes. *Proteins Struct. Funct. Bioinf.* **2008**, *73*, 765–783.
- S11. Olsson, M.H.M.; Sondergaard, C.R.; Rostkowski, M.; Jensen, J.H. PROPKA3: Consistent Treatment of Internal and Surface Residues in Empirical pK_a Predictions. *J. Chem. Theory Comput.* **2011**, *7*, 525–537.
- S12. Sugio, S.; Kashima, A.; Mochizuki, S.; Noda, M.; Kobayashi, K. Crystal structure of human serum albumin at 2.5 Å resolution. *Protein Eng.* **1999**, *12*, 439–446.
- S13. Stoll, S.; Schweiger, A. EasySpin, a comprehensive software package for spectral simulation and analysis in EPR. *J. Magn. Reson.* **2006**, *178*, 42–55.
- S14. Reichenwallner, J.; Thomas, A.; Nuhn, L.; Johann, T.; Meister, A.; Frey, H.; Hinderberger, D. Tunable dynamic hydrophobic attachment of guest molecules in amphiphilic core-shell polymers. *Polym. Chem.* **2016**, *7*, 5783–5798.
- S15. Nelder, J.A. Inverse Polynomials, a Useful Group of Multi-Factor Response Functions. *Biometrics* **1966**, *22*, 128–141.
- S16. Gumbel, E.J. Bivariate Logistic Distributions. *J. Am. Stat. Assoc.* **1961**, *56*, 335–349.
- S17. Steinhoff, H.J.; Savitsky, A.; Wegener, C.; Pfeiffer, M.; Plato, M.; Möbius, K. High-field EPR studies of the structure and conformational changes of site-directed spin labeled bacteriorhodopsin. *Biochim. Biophys. Acta, Bioenerg.* **2000**, *1457*, 253–262.